Bottom-Up Development of Nanoimprinted PLLA Composite Films with Enhanced Antibacterial Properties for Smart Packaging Applications

Eleni Psochia [1], **Lazaros Papadopoulos [1]**, **Dimitrios J. Gkiliopoulos [2]**, **Achille Francone [3]**, **Maria-Eirini Grigora [4]**, **Dimitrios Tzetzis [4]**, **Joana Vieira de Castro [5,6]**, **Nuno M. Neves [5,6]**, **Konstantinos S. Triantafyllidis [2]**, **Clivia M. Sotomayor Torres [3,7]**, **Nikolaos Kehagias [3,8]** and **Dimitrios N. Bikiaris [1,*]**

1. Laboratory of Polymer Chemistry and Technology, Department of Chemistry, Aristotle University of Thessaloniki, 54124 Thessaloniki, Greece; epsochia@gmail.com (E.P.); lazaros.geo.papadopoulos@gmail.com (L.P.)
2. Laboratory of Chemical and Environmental Technology, Department of Chemistry, Aristotle, University of Thessaloniki, 54124 Thessaloniki, Greece; dgiliopo@chem.auth.gr (D.J.G.); ktrianta@chem.auth.gr (K.S.T.)
3. Catalan Institute of Nanoscience and Nanotechnology (ICN2), CSIC and BIST, Campus UAB, Bellaterra, 08193 Barcelona, Spain; achille.francone@icn2.cat (A.F.); clivia.sotomayor@icn2.cat (C.M.S.T.); n.kehagias@inn.demokritos.gr (N.K.)
4. Digital Manufacturing and Materials Characterization Laboratory, School of Science and Technology, International Hellenic University, Thermi, 57001 Thessaloniki, Greece; megrigora@gmail.com (M.-E.G.); d.tzetzis@ihu.edu.gr (D.T.)
5. 3B's Research Group, I3B's—Research Institute on Biomaterials, Biodegradables and Biomimetics, University of Minho, Headquarters of the European Institute of Excellence on Tissue Engineering and Regenerative Medicine AvePark, Zona Industrial da Gandra, Barco, 4805-017 Guimarães, Portugal; joana.castro@i3bs.uminho.pt (J.V.d.C.); nuno@i3bs.uminho.pt (N.M.N.)
6. ICVS/3B's—PT Government Associate Laboratory, University of Minho, 4710-057/4805-017 Braga/Guimarães, Portugal
7. ICREA, Pg. Lluís Companys 23, 08010 Barcelona, Spain
8. Institute of Nanoscience and Nanotechnology, NCSR Demokritos, 15341 Ag. Paraskevi, Greece
*   Correspondence: dbic@chem.auth.gr; Tel.: +30-2310-997-812

Abstract: In this work, polymer nanocomposite films based on poly(L-lactic acid) (PLLA) were reinforced with mesoporous silica nanoparticles, mesoporous cellular foam (MCF) and Santa Barbara amorphous-15 (SBA). PLLA is a biobased aliphatic polyester, that possesses excellent thermomechanical properties, and has already been commercialized for packaging applications. The aim was to utilize nanoparticles that have already been established as nanocarriers to enhance the mechanical and thermal properties of PLLA. Since the introduction of antibacterial properties has become an emerging trend in packaging applications, to achieve an effective antimicrobial activity, micro/nano 3D micropillars decorated with cone- and needle-shaped nanostructures were implemented on the surface of the films by means of thermal nanoimprint lithography (t-NIL), a novel and feasible fabrication technique with multiple industrial applications. The materials were characterized regarding their composition and crystallinity using Fourier transform infrared spectroscopy (FT-IR) and X-ray diffraction (XRD), respectively, and their thermal properties using differential scanning calorimetry (DSC) and thermogravimetric analysis (TGA). Their mechanical properties were examined by the nanoindentation technique, while the films' antimicrobial activity against the bacteria *Escherichia coli* and *Staphylococcus aureus* strains was tested in vitro. The results demonstrated the successful production of nanocomposite PLLA films, which exhibited improved

mechanical and thermal properties compared to the pristine material, as well as notable antibacterial activity, setting new groundwork for the potential development of biobased smart packaging materials.

1. Introduction

Scientific research has been directed towards biobased polymers, as the environmental impact of petroleum-based materials has become a matter of great concern in modern societies [1]. To this end, renewable resources like proteins, oils, and carbohydrates have been employed to produce biodegradable and sustainable polymeric and nanocomposite materials [2,3]. In this context, packaging industries have recently focused on the development of environmentally-friendly, "smart" packaging materials which, at the same time can include aspects like antimicrobial protection and/or hydrophobicity (tamper-proofing), providing extended shelf life and fulfilling consumer demands and therefore maximizing profits [4]. Such properties are usually achieved by utilization of nanofillers, which can serve both as reinforcing agents and nanocarriers of antimicrobial substances [5].

Poly(L-lactic acid) (PLLA), the polymer of interest here, is a biobased and compostable aliphatic polyester, and its monomer, DL-lactide is produced on a mass scale by the microbial fermentation of agricultural by-products [6–9]. Owing to its beneficial characteristics, such as good mechanical properties, transparency, biodegradability, and biocompatibility, PLLA is widely used in many industrial fields e.g., in the pharmaceutics, biomedicine, and textile industries [2,8,10–13]. Having been classified as a safe (Generally Recognized as Safe-GRAS) material by the Food and Drug Administration-FDA, it is also currently used in food packaging applications [14], and also has strong potential as a "smart" packaging material. PLLA nanocomposites can play a significant role in this sector, because, in addition to possessing improved features compared to the neat polyester, such as heat sealability and gas barrier properties [1], they also introduce new characteristics such as antioxidant and antimicrobial properties, when encapsulated with the respective agents [2,15,16].

In order to load a polymer matrix with active agents, porous nanomaterials of determined structure are preferred. Among those, ordered mesoporous silica nanoparticles (MSNs) maintain a major position, as they have been screened successfully for potential use in drug delivery systems [17–19]. Lately, nanoparticles of this class with different geometries have been used to create smart packaging materials with prominent results. In particular, Santa Barbara amorphous (SBA-15) and mesoporous cellular foam (MCF) nanoparticles, with 2D hexagonal arrangement of cylindrical pores and 3D porous system of spherical structure, respectively, [17,20,21] were used as nanocarriers for chemical preservatives to develop polymeric matrices with antimicrobial properties [22–24]. Ideally, the next step towards more consumer-friendly materials would be the incorporation of natural ingredients that exhibit such properties, such as essential oils [25–28]. However, their volatile nature requires further optimization of such procedure, as their effective concentration decreases during high temperature processing [29–31].

An alternative approach to developing substrates with antibacterial properties lies in the formation of topographical features in micro- or nanoscales [32]. Such nanosized topographies can easily be fabricated by t-NIL [33,34]. Nanostructured polymeric films can exhibit hydrophobic and antibacterial characteristics, making them suitable for applications in electronics, optics, and especially biomedicine, where such properties pave the way for novel therapeutic strategies [24,35–37]. For example, Nerantzaki [32] et al. showed that the synergistic effect of proper nanoinclusions combined with nanotopography can result in materials with superior antimicrobial properties. Based on the above, it is only natural to assume that applying this strategy to materials intended for packaging applications would be beneficial for this industry as well.

In this work, we examine the possibility of developing a fully biobased nanocomposite material with the prospect of using it in smart packaging. To this end, MCF and SBA-15 nanoparticles, which due to their porous system can potentially act as nanocarriers and mechanical properties enhancers, were prepared and incorporated in PLLA biobased polyester. The nanocomposites were then formed into films and t-NIL was used to implement micro- and nanosized topographies. Different concentrations of the nanoparticles were used to prepare materials of different properties, namely 1, 2.5, and 5 wt%, and the produced films were then characterized as to their structural, thermal, and mechanical properties. Moreover, their antibacterial activity against *E. coli* and *S. aureus* was also examined, with promising results.

2. Experimental Section

2.1. Materials

Pluronic P-123 (poly(ethylene glycol)-block-poly(propylene glycol)-block-poly(ethylene glycol) triblock copolymer with average Mn ~5800, 1,2,3-trimethylbenzene (TMB), tetraethyl orthosilicate (TEOS), and ammonium fluoride (NH_4F) were acquired by Sigma-Aldrich Chemical Co. (Steinheim, Germany). PLLA of molecular weight ~63 kg/mol and ~96% L-lactide composition was kindly supplied by Plastika Kritis S.A (Iraklion, Greece). Chloroform ($CHCl_3$) (99.5%) was obtained from Chem-Lab NV (Zedelgem, Belgium).

2.2. Synthesis of MCF and SBA-15 Silica

The mesostructured cellular foam (MCF) silica was synthesized via a self-assembly method using non-ionic surfactant pluronic P-123 as the structure directing agent, 1,2,3-trimethylbenzene (TMB) as co-surfactant, ammonium fluoride (NH_4F) as mineralizing agent, and tetraethyl orthosilicate (TEOS) as the silica source, in acidic pH conditions [24,35]. Typically, P-123 was diluted in aqueous HCl 1.6 M followed by the addition of NH_4F and TMB. After 1 h at 40 °C, TEOS was added and the reacting mixture was further stirred for 20 h at 40 °C. The mixture was then heated in an autoclave at 100 °C for 24 h. Finally, the solid products were recovered by filtration and washed with deionized water. The organic templates were removed by calcination in air at 500 °C, for 8 h, with a heating rate of 1 °C/min.

The SBA-15 (Santa Barbara amorphous) mesoporous silica was prepared according to previously reported methods [20,36,37]. In a typical procedure, pluronic P-123 was dissolved in aqueous 1M HCl solution at pH ≤ 1 at 35 °C. Subsequently, TEOS was added and the solution was stirred for another 1 h. The resulting suspension was aged under static conditions at 35 °C for 48 h, while the molar ratio of the synthesis mixture was 1 TEOS:0.018 P123:3.3HCl:97.5 H_2O. The solid products were isolated by filtration and washed with deionized water. Calcination was carried out in air at 550 °C, for 6 h, with a heating rate of 1 °C /min, to combust the organic template and produce the mesoporous silica.

2.3. Nanocomposite Preparation

A total of six PLLA nanocomposites, containing 1, 2.5, and 5 wt% of MCF and SBA-15, respectively, were prepared via melt mixing [38]. PLLA and the respective nanoparticles were mixed in a twin-screw corotating melt mixer for 10 min at 180 °C with a rotating speed of 30 rpm.

2.4. Preparation of Films by Spin-Coating

Thin films of neat PLLA and the prepared nanocomposites were produced by spin coating [39,40]. Specifically, each material was dissolved in chloroform, in order to obtain a 10% *w/v* solution. A drop of the solution was placed on silicon substrates, previously cut into 2 cm × 2 cm pieces, and spin-coated at a speed of 500 rpm/min for 1 min. With this procedure, seven polymeric films were fabricated—neat PLLA, PLLA/MCF 1 wt%, PLLA/MCF 2.5 wt%, PLLA/MCF 5 wt%, PLLA/SBA-15 1 wt%, PLLA/SBA-15 2.5 wt%, and PLLA/SBA-15 5 wt%.

2.5. Patterning of PLLA Nanocomposite Films by NIL

Before imprint, the spin-coated silicon substrates were heated at 100 °C for 15 min to ensure solvent evaporation. Afterwards, thermal NIL was performed using a commercial desktop 4-inch Compact Nanoimprint (CNI) tool, that was supplied from NIL Technology ApS. Polydimethylsiloxane (PDMS) stamps were used to achieve a soft release and a successful replication. The polymeric substrate and the stamp were heated to 210 °C, under a pressure of 5 bars for 10 min. After cooling to below 40 °C, the PDMS mold was separated from the polymeric material [32].

2.6. Nanoparticle Characterization Methods

2.6.1. Fourier Transform-Infrared Spectroscopy (FT-IR)

FT-IR spectra of the silica nanoparticles and the nanocomposite PLLA films were obtained on a PerkinElmer FT-IR spectrometer (PerkinElmer, Waltham, MA, USA), model SPECTRUM 1000 (Spectrum 1). The silica nanoparticles' spectra were obtained using KBr pellets, while the nanocomposite materials' measurements were conducted using thin films. Infrared (IR) absorbance spectra were obtained between 450 and 4000 cm^{-1} at a resolution of 4 cm^{-1} using 16 co-added scans. All spectra presented are baseline corrected and normalized.

2.6.2. N_2 Porosimetry

Nitrogen adsorption-desorption experiments at −196 °C were conducted to assess the surface area (multi-point Brunauer–Emmett–Teller (BET) method), total pore volume (at P/P_o = 0.99), and pore size distribution (Barrett–Joyner–Halenda (BJH) method using adsorption data) of the MCF and SBA-15 silica nanoparticles. The synthesized silicas were previously outgassed at 150 °C for 16 h under 6.6×10^{-9} mbar vacuum using an automatic volumetric sorption analyzer (Autosorb-1MP, Quantachrome, FL, USA).

2.6.3. Thermogravimetric Analysis (TGA)

Thermogravimetric analysis of the mesoporous silicas and the prepared films was carried out with a SETARAM (Lyon, France) SETSYS TG-DTA 16/18. Samples (6.0 ± 0.2 mg) were placed in alumina crucibles. An empty alumina crucible was used as reference. The samples were heated from ambient temperature to 600 °C in a 50 mL/min flow of N2 at heating rate of 20 °C/min.

2.7. Characterization of the Prepared Films

2.7.1. Scanning Electron Microscopy (SEM)

The morphology of the imprinted materials was examined using a scanning electron microscope (SEM), type FEI Quanta 650 FEG. All the studied samples were coated with carbon black to avoid charging under the electron beam.

2.7.2. X-ray Diffraction (XRD)

XRD analysis was performed on the PLLA/MCF and PLLA/SBA-15 films over the 5–45° 2θ range, using a MiniFlex II diffractometer Rigaku Co. (Rigaku Company, Tokyo, Japan) with Bragg–Brentano geometry (θ,2θ) and a Ni-filtered CuKa radiation (λ = 0.154 nm).

2.7.3. Differential Scanning Calorimetry (DSC)

For the DSC measurements a Perkin–Elmer, Pyris Diamond DSC differential scanning calorimeter, previously calibrated with indium and zinc standards, was employed. To determine the thermal properties of the nanocomposite films after t-NIL, a sample of about 5 mg was used for each test, placed in sealed aluminum pan and heated to 200 °C at a heating rate of 20 °C/min.

2.7.4. Nanoindentation

Experiments were carried out using a dynamic ultra-micro-hardness tester (DUH-211; Shimadzu Co., Kyoto, Japan) fitted with a triangular pyramid indenter tip (Berkovich indenter) with a tip radius of 100 nm. The indentations made on the surface of the nanocomposites under study appeared as an equilateral triangle. After contact of the indenter with the surface, this was driven into the surface until a peak load of 3 mN was reached. The peak load was held for 3 s (in order to minimize the effect of viscoelastic deformation of the specimen, notably creep, on property measurements) and then the indenter was unloaded, to a load of zero. Five measurements were conducted on each specimen and the results were expressed as mean ± standard deviation.

2.7.5. Antibacterial Activity

The antibacterial activity of PLLA nanocomposite films, before and after patterning, was evaluated. The protocol used was the swab assay that is a method based on touch transfer assay [41]. This assay allows for evaluation of the attachment of viable bacteria directly from the surface of films and achievement of a homogenous and well-distributed inoculum on the surface of the films.

Bacterial strains of *E. coli* (BL21) and *S. aureus* (ATCC 25923) were used as the model Gram-negative and Gram-positive bacteria, respectively. Bacteria (*E. coli* and *S. aureus*) were grown at 37 °C, 200 rpm, 18–24 h in 50 mL of sterile tryptic soy broth (TSB) medium. Prior to inoculation, strains were sub-cultured into fresh TSB at 1:50 dilution and incubated for approximately 2 h at 37 °C, 200 rpm. Bacteria were collected by centrifugation (2000 rpm, 10 min) and resuspended in PBS. The number of bacteria was spectrophotometrically adjusted to O.D.600 nm = 0.5 (equivalent to 5×10^8 CFU/mL). Then, a cotton swab soaked on the bacterial suspension (5×10^4 CFU/mL) was used to spread (vertically and horizontally) the bacterial suspension. The films were allowed to dry for 10 min. Finally, the contact plates were pressed against the films for 10 s, incubated at 37 °C for 18–24 h, and the resulting colonies were counted.

3. Results and Discussion

3.1. Nanoparticle Characterization

3.1.1. FT-IR

As observed in Figure 1, both MCF and SBA-15 exhibited one broad band at 3453 cm^{-1} which can be attributed to –O–H stretching vibrations of absorbed water molecules, while the respective bending vibration mode could also be identified at 1633 cm^{-1}. The intense band at 1090 cm^{-1} is attributed to Si–O bonds, while the one at 802 cm^{-1} to Si–O–Si, all being characteristic bands of MCF and SBA-15, which proves that the corresponding mesoporous nanoparticles had been successfully prepared [19,24].

3.1.2. Porosity

The porous characteristics of the parent MCF and SBA-15 silica were studied by N$_2$ porosimetry at −196 °C and the respective data are presented in Figure 2 and Table 1. The adsorption isotherm of the parent MCF silica is of type IV according to the IUPAC classification [42], typical for such types of ordered mesoporous materials. It is well known that MCF exhibits cellular pore morphology of relatively large size pores giving a foam-like texture [43]. MCF exhibits a specific surface area (BET method) of 837 m^2/g and a high total pore volume of 1.56 cc/g. Its average pore size is 18.5 nm and it could be ideal for an antimicrobial agent adsorption.
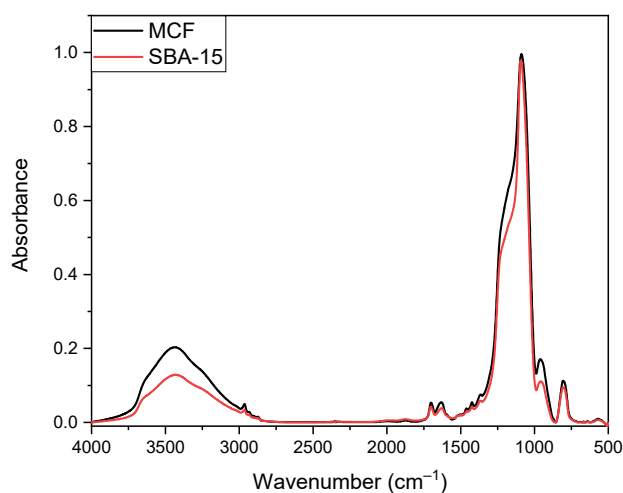
Figure 1. FT-IR spectra of the synthesized mesoporous cellular foam (MCF) and Santa Barbara amorphous (SBA-15) nanoparticles.
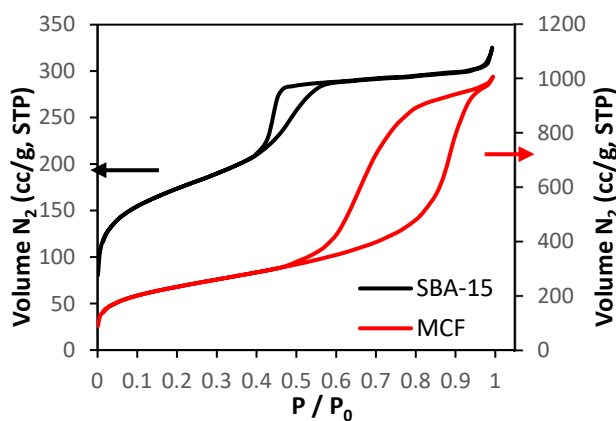

Figure 2. N_2 adsorption–desorption isotherms of the parent MCF and SBA-15 mesoporous silica.

Table 1. Porosity data of mesoporous silicas MCF and SBA-15.

Material	Specific Surface Area (m^2/g)	Total Pore Volume $P/P_0 = 0.99$ (cm^3/g)	Average Pore Diameter (nm)	Window Diameter (nm)
SBA-15	619	0.5	4	-
MCF	837	1.56	18.5	6.1

The adsorption isotherm of the parent SBA-15 silica is of type IV according to the IUPAC classification [42], typical for such types of ordered mesoporous materials. The specific surface area of SBA-15 (BET method) is 619 m^2/g, while its total pore volume 0.5 cc/g and its pore diameter 4 nm.

3.1.3. TGA Analysis

The synthesized silicas' thermal stability was evaluated, using TGA analysis. The results demonstrate that both MCF and SBA-15 nanoparticles showed only a slight mass loss in the range of temperature of 40–100 °C which corresponds to the removal of the absorbed humidity (Figure 3) [44]. The weight loss recorded at this stage, was about 4% and 6% for MCF and SBA-15 nanoparticles, respectively. It was clearly exhibited that up to 500 °C, the silicas do not present any significant mass loss, indicating that their decomposition starts at higher temperatures [24].
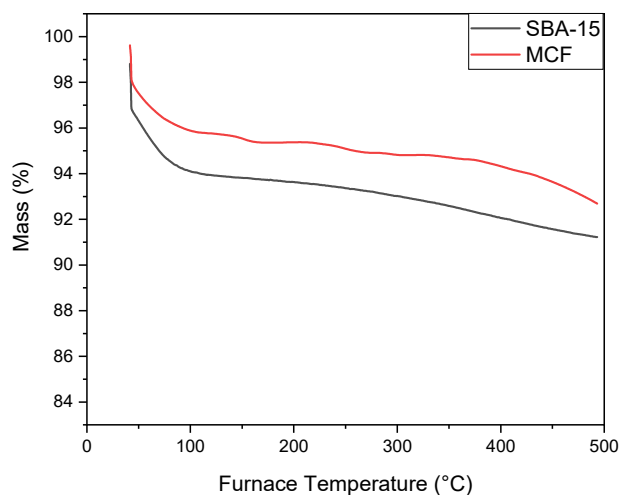
Figure 3. Thermogravimetric analysis (TGA) thermograms of the synthesized MCF and SBA-15 nanoparticles.

3.2. Characterization of the Imprinted Nanocomposite Films

3.2.1. Morphological Study of Micro- and Nanosized Topographies

Hierarchical nanostructures were formed on the surface of the spin-coated nanocomposite films by means of thermal NIL, aimed at providing them with antibacterial properties. In order to confirm the successful formation of the nanostructures, the films' surface morphology was examined with scanning electron microscopy (SEM). In Figure 4 we demonstrate three-dimensional (3D) hierarchical domains on the surface of PLLA films. It can be seen that micropillars with 5 μm width and 5 μm height, decorated with cone- and needle-shaped nanostructures on the top surface, and with 600 nm width, were successfully fabricated on the surface of the nanocomposite PLLA films.
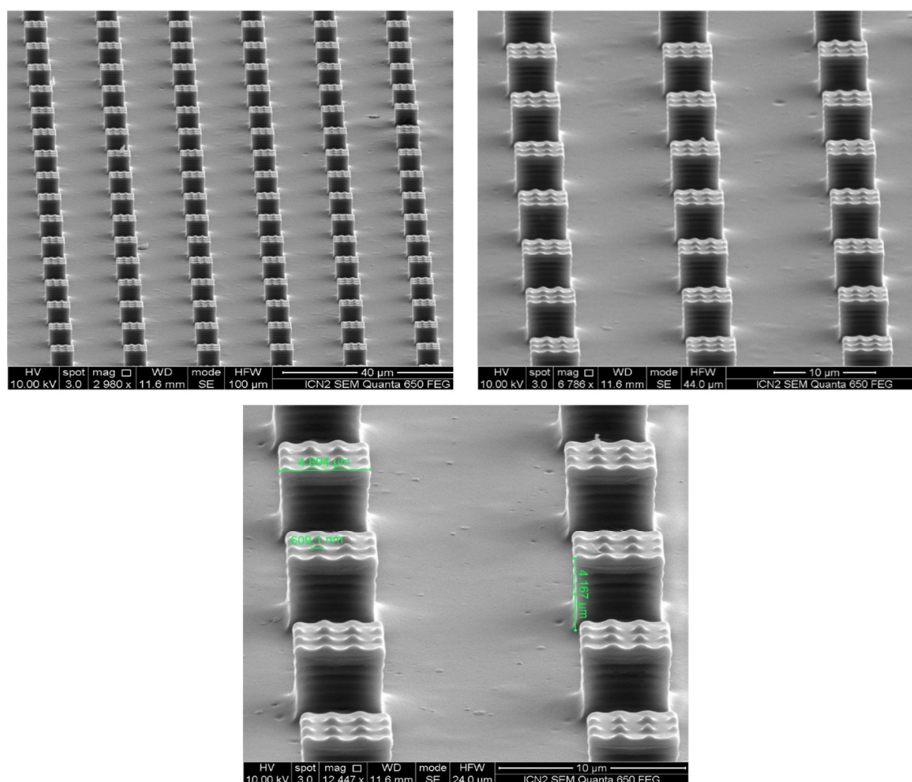

Figure 4. SEM images of the hierarchical nanostructured nanocomposite poly(L-lactic acid) (PLLA) surface at different magnifications.

As SEM observations confirm, all nanocomposite films had fine morphological features while the nanostructures were homogenously dispersed throughout the surface. In addition, the presence of MCF and SBA-15 did not affect the surface morphology and the topographical features of the PLLA films since the hierarchical domains were perfectly shaped and homogenously distributed in the polymer matrix.

3.2.2. Fourier Transform-Infrared Spectroscopy (FT-IR)

FT-IR was used to determine the chemical composition of the prepared materials. In Figure 5, all the characteristic bands of PLLA were present—two bands at 3000 and 2850 cm^{-1} owing to the stretching vibrations of –C–H and one sharp, characteristic band at 1760 cm^{-1} due to stretching vibration of –C=O bonds. The bands at 1500–1400 cm^{-1} and at 1100–1000 cm^{-1} are associated with the bending and stretching vibrations of –C–H and –C–O bonds, respectively [32]. In the spectra of the nanocomposites, there is an increase in the intensity of the signal at 1090 cm^{-1}, derived from the mutual absorbance of PLLA and the nanoparticles at the specific wavenumber. This is evidence of the successful incorporation of the silicas into the polymer matrix. The nanocomposites' films obtained FT-IR spectra are presented in detail in Supplementary Materials (Figure S1).
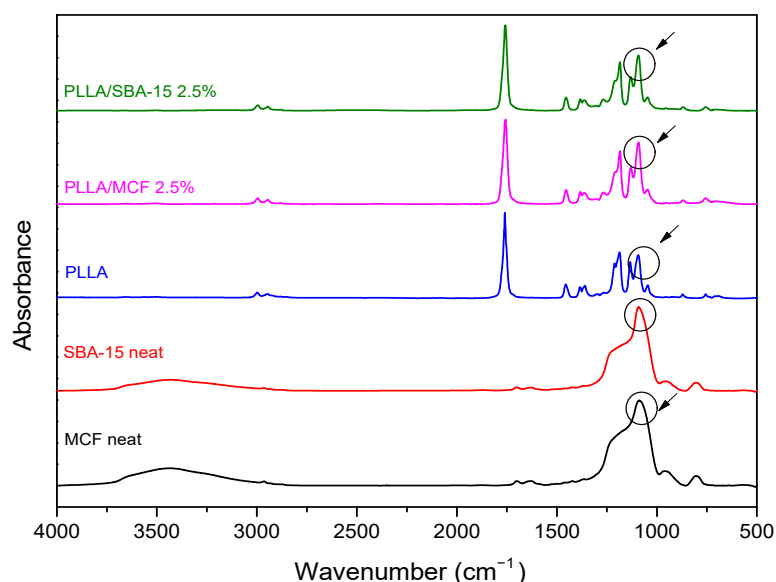

Figure 5. FT-IR spectra of neat MCF, neat SBA-15, neat PLLA, PLLA/MCF 2.5 wt%, and PLLA/SBA-15 2.5 wt%.

3.2.3. X-ray Diffraction (XRD)

To evaluate if the thermal treatment of t-NIL affected the crystallinity of the prepared films, XRD was employed. The diffractograms are presented in Figure 6, and they exhibit one broad peak at 16.8° indicative of their amorphous nature. Considering that the materials were prepared via spin coating, their initial amorphous character was expected, as the solvent's rapid evaporation does not favor the polymer chains' arrangement and therefore hinders its crystallization [32]. Moreover, t-NIL does not seem to have an impact on the materials' crystallinity, since they remain amorphous after their imprinting treatment. Finally, reflections derived from the silica nanoparticles are not to be expected in the measurements' range, since MCF is amorphous [45] and SBA-15 reflects at lower angles [45,46].
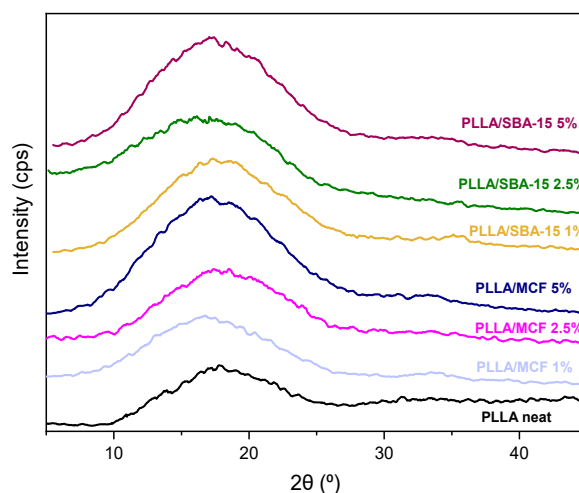
Figure 6. XRD patters of neat PLLA, neat MCF, neat SBA-15, PLLA/MCF 2.5 wt% and PLLA/SBA-15 2.5 wt%.

3.2.4. Differential Scanning Calorimetry (DSC)

In addition to XRD analysis, DSC measurements were also conducted, to further elaborate on the thermal properties of the nanopatterned materials. The obtained results are presented in Figure 7. The α-relaxation observed as an endothermic phenomenon right after T_g, along with the strong cold crystallization further support the XRD findings. The addition of the nanoparticles decreased the mobility of the polymer chains in the nanocomposites, but their effect was not very pronounced as the glass transition temperatures increased by 2–3 °C. However, the fillers acted as crystallization nuclei as the lower cold crystallization temperature (T_{cc}) recorded clearly demonstrates [24]. Overall, the thermal properties of the nanocomposites were improved compared to the pristine material, with an increased glass transition and a lower crystallization temperature. A more detailed analysis of the thermal properties and the effect of the silicas on the crystallization of the materials can be found on our recent publication [38]. The values of the samples' characteristic temperatures are summarized in Table 2.
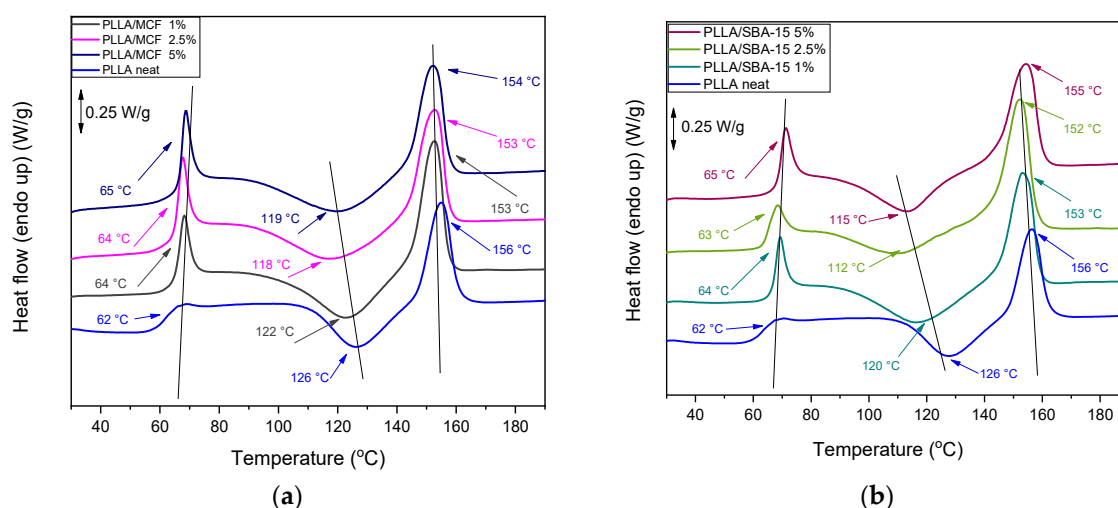

Figure 7. Differential scanning calorimetry (DSC) curves of PLLA and its nanocomposites obtained during heating with 20 °C/min. (**a**) DSC thermograms of PLLA/MCF nanocomposites and (**b**) DSC thermograms of PLLA/SBA-15 nanocomposites

Table 2. Thermal properties of neat PLLA and its nanocomposite films.

Sample	T_g (°C)	T_{cc} (°C)	ΔH_{cc} (J/g)	T_m (°C)	ΔH_m (J/g)
Neat PLLA	62	126	17.1	156	18.9
PLLA/MCF 1%	64	122	23.1	153	23.6
PLLA/MCF 2.5%	64	118	21.6	153	23
PLLA/MCF 5%	65	119	22.4	154	24.7
PLLA/SBA-15 1%	64	120	23.3	153	25.4
PLLA/SBA-15 2.5%	63	112	20.8	152	24
PLLA/SBA-15 5%	65	115	24.2	155	26.1

3.2.5. Thermogravimetric Analysis (TGA)

The thermal stability of the materials was also assessed, by means of TGA. From the results presented in Figure 8, it is clear that the materials' degradation was impeded by the nanoinclusions, since the mass loss of the nanocomposites started at higher temperatures compared to neat PLLA and the T_{max} also increases [47,48]. It is worth noting that all the nanocomposite films presented an increased mass residue compared to neat PLLA films. This increase can be associated with two different facts—firstly, after the nanofillers' addition into the polymeric matrix, it is more difficult for the macromolecular chains to move while some of them are even immobilized in the so-called rigid amorphous fraction (RAF) [6,49,50], resulting in a larger final mass residue and secondly, MCF and SBA-15 nanoparticles' degradation does not start in the temperature range where the measurements were conducted [24], as previously showed from the nanoparticles' TGA analysis. Therefore, part of the final residual mass corresponded to that of the incorporated nanoparticles, leading to a total mass increase. Taking the above-mentioned facts into consideration, it is clear that the thermal stability of the produced materials was improved. The values for the characteristic temperatures and mass residues at 500 °C are summarized in Table 3, while DTG curves are presented in Supplementary Materials (Figure S3).
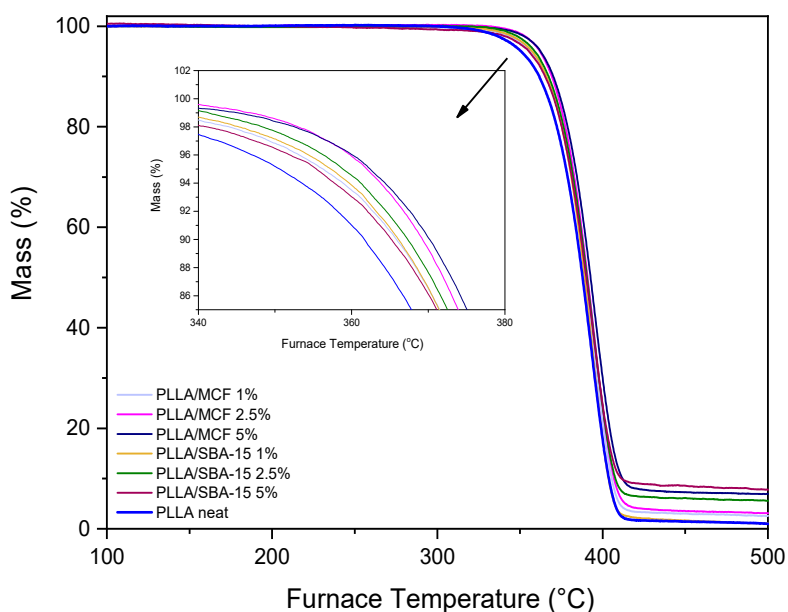

Figure 8. TGA thermograms of PLLA and its nanocomposites.

Table 3. Degradation temperatures of neat PLLA and PLLA nanocomposites.

Sample	$T_{d,5\%}$ (°C)	$T_{d,10\%}$ (°C)	$T_{d,max}$ (°C)	R_{500} (%)
Neat PLLA	350	361	413	1.8
PLLA/MCF 1%	355	365	419	3.4
PLLA/MCF 2.5%	360	369	423	4.5
PLLA/MCF 5%	361	369	426	7.8
PLLA/SBA-15 1%	356	365	420	2
PLLA/SBA-15 2.5%	358	366	423	6.1
PLLA/SBA-15 5%	358	366	426	8

3.2.6. Nanoindentation Tests

To investigate the mechanical properties of the prepared materials, nanoindentation tests were conducted to compare their elastic modulus and hardness. This method is based on measuring the load as a function of the penetration depth [51]. The loading–unloading curves show no discontinuities or steps indicating the absence of any cracks during indentation, while PLLA/MCF 1 and 2.5 wt% showed smaller creep at the peak force. The indentation depths at the peak load range was between approximately 0.6 and 1.1 μm for all nanocomposite films. The loading–unloading nanoindentation curves can be found in Supplementary Materials (Figure S2). Results showed that the addition of 1 and 2.5 wt% MCF nanoparticles led to a dramatic increase in indentation hardness and elastic modulus, since silica nanoparticles are materials of increased hardness compared to polymers [52] and consequently their dispersion into the polymer matrix resulted in materials of increased mechanical strength. Regarding the SBA-15 nanoparticles, while the elastic modulus was increased for both 1 and 2.5 wt% concentrations, the hardness increase was only significant in the case of 2.5 wt%. When filler incorporation increased to 5 wt%, in both materials the mechanical properties deteriorated compared to those of 2.5 wt%, which is probably an indication of agglomerate formation. The nanoindentation results are presented in detail in Table 4.

Table 4. Hardness and elastic modulus values of neat PLLA, PLLA/MCF, and PLLA/SBA-15 nanocomposite films.

Sample	Hardness (MPa)	St Dev	Elastic Modulus (MPa)	St Dev
Neat PLLA	108	2	4580	188
PLLA/MCF 1%	193	20	6974	390
PLLA/MCF 2.5%	201	23	7035	366
PLLA/MCF 5%	85	7	4285	156
PLLA/SBA-15 1%	105	17	5125	371
PLLA/SBA-15 2.5%	126	13	5890	54
PLLA/SBA-15 5%	110	21	5720	135

3.2.7. Antibacterial Activity Analysis

While trying to develop materials for smart-packaging, the most fundamental challenge is to eliminate or substantially reduce the ability of bacteria to adhere to material surfaces and to prevent biofilm formation. The t-NIL technique is a viable strategy to create micro- or nanometer-scaled topographies like slopes walls, columns etc., on materials surfaces, that drastically reduce the available area for the bacteria to attach compared with their smooth unpatterned equivalents [53].

The bactericidal properties of the nanopatterned films were examined by incubating two species of bacteria on each film surface for periods up to 24 h and assessing their bacterial viability. Specifically, Gram-negative *E. coli* and Gram-positive *S. aureus* were separately grown on the surface of the nanocomposite films PLLA/MCF 2.5 wt%, and PLLA/SBA-15 2.5 wt%.

As shown in Figure 9, lower cell densities were measured on the nanostructured surfaces (PLLA/SBA-15 2.5 wt% and PLLA/MCF 2.5 wt%) compared to the unpatterned films. Moreover,

S.aureus presented the lowest growth on the surfaces with hierarchical structure (PLLA/SBA-15 2.5 wt% TOP and PLLA/MCF 2.5 wt% TOP) compared to its respective ones without topography (PLLA/SBA-15 2.5 wt% NO TOP and PLLA/MCF 2.5 wt% NO TOP). Similar results were obtained by studying the bacterial growth of *E. coli* on the surface of the above-mentioned films, with nanopatterned PLLA/MCF 2.5 wt% presenting the best antibacterial activity. Taking these results into consideration, it can be concluded that the nanocomposite PLLA films' surfaces enhanced with micro/nano-topographical features inhibited significant bacterial growth compared to those with flat or unpatterned surfaces, as the available area for bacteria attachment w reduced [32,33,54,55].
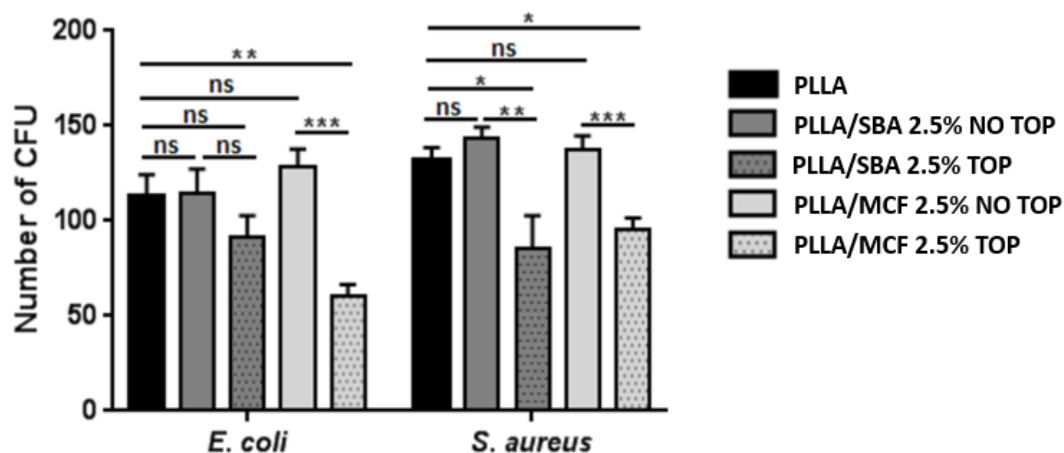

Figure 9. Number of CFU formed on the surface of the films prepared in this work (ns; non susceptible, *; low CFU number, **; high CFU number, ***; very high CFU number).

4. Conclusions

In this study, biobased nanoimprinted films of PLLA nanocomposites were prepared and studied. Home-made porous silica nanoparticles were prepared and melt-mixed with pristine PLLA, and the materials were spin-coated to form thin films containing 1, 2.5, and 5 wt% MCF and SBA-15 nanoparticles, respectively. To introduce antibacterial activity to their surfaces, the films were nanopatterned with t-NIL. Evaluation of the films' properties showed that the combination of techniques used, led to the successful synthesis of amorphous nanocomposite materials. The thermal and mechanical properties of the materials could be altered on-demand, depending on the amount of filler incorporated in the matrix, as they were found to act both as reinforcing and nucleating agents. In addition, all nanocomposite films exhibited improved thermal stability, as degradation started at increased temperatures and higher mass residues were achieved with increased nano silicate concentration. Finally, the nanostructures created from t-NIL were found to significantly inhibit the attachment of *E. coli* and *S. aureus* on the PLLA surfaces. This suggests that t-NIL is a viable and promising technique for designing materials with antibacterial properties. The fact that mesoporous home-made nanoparticles, that are known carriers for antimicrobial agents, can also act as reinforcing agents for a biobased packaging material, indicates that novel technological pathways are available to reach sustainable smart packaging.

Conflicts of Interest: The authors declare no conflict of interest.

References

1. Jamshidian, M.; Tehrany, E.A.; Imran, M.; Jacquot, M.; Desobry, S. Poly-Lactic Acid: Production, applications, nanocomposites, and release studies. *Compr. Rev. Food Sci. Food Saf.* **2010**, *9*, 552–571. [CrossRef]
2. Lopez-Rubio, A.; Gavara, R.; Lagaron, J.M. Bioactive packaging: Turning foods into healthier foods through biomaterials. *Trends Food Sci. Technol.* **2006**, *17*, 567–575. [CrossRef]
3. Alfei, S.; Schito, A.M.; Zuccari, G. Biodegradable and Compostable Shopping Bags under Investigation by FTIR Spectroscopy. *Appl. Sci.* **2021**, *11*, 621. [CrossRef]
4. Ahmed, I.; Lin, H.; Zou, L.; Brody, A.L.; Li, Z.; Qazi, I.M.; Pavase, T.R.; Lv, L. A comprehensive review on the application of active packaging technologies to muscle foods. *Food Control* **2017**, *82*, 163–178. [CrossRef]
5. Alfei, S.; Marengo, B.; Zuccari, G. Nanotechnology application in food packaging: A plethora of opportunities versus pending risks assessment and public concerns. *Food Res. Int.* **2020**, *137*, 109664. [CrossRef] [PubMed]
6. Papageorgiou, G.Z.; Terzopoulou, Z.; Bikiaris, D.; Triantafyllidis, K.S.; Diamanti, E.; Gournis, D.; Klonos, P.; Giannoulidis, E.; Pissis, P. Evaluation of the formed interface in biodegradable poly(l-lactic acid)/graphene oxide nanocomposites and the effect of nanofillers on mechanical and thermal properties. *Thermochim. Acta* **2014**, *597*, 48–57. [CrossRef]
7. Gruber, P.; O'Brien, M. Polylactides "NatureWorks®PLA". *Biopolym. Online* **2002**, 235–239. [CrossRef]
8. Gupta, A.P.; Kumar, V. New emerging trends in synthetic biodegradable polymers—Polylactide: A critique. *Eur. Polym. J.* **2007**, *43*, 4053–4074. [CrossRef]
9. Hong, C.L.S. An Overview of the Synthesis and Synthetic Mechanism of Poly(Lactic acid). *Mod. Chem. Appl.* **2014**, *2*. [CrossRef]
10. Lasprilla, A.J.R.; Martinez, G.A.R.; Lunelli, B.H.; Jardini, A.L.; Filho, R.M. Poly-lactic acid synthesis for application in biomedical devices—A review. *Biotechnol. Adv.* **2012**, *30*, 321–328. [CrossRef]
11. Vert, M.; Schwarch, G.; Coudane, J. Present and Future of PLA Polymers. *J. Macromol. Sci. Part A* **1995**, *32*, 787–796. [CrossRef]
12. Ataman-Önal, Y.; Munier, S.; Ganée, A.; Terrat, C.; Durand, P.Y.; Battail, N.; Martinon, F.; Le Grand, R.; Charles, M.H.; Delair, T.; et al. Surfactant-free anionic PLA nanoparticles coated with HIV-1 p24 protein induced enhanced cellular and humoral immune responses in various animal models. *J. Control. Release* **2006**, *112*, 175–185. [CrossRef] [PubMed]
13. Shen, W.; Zhang, G.; Li, Y.L.; Fan, G. Effects of the glycerophosphate-polylactic copolymer formation on electrospun fibers. *Appl. Surf. Sci.* **2018**, *443*, 236–243. [CrossRef]
14. Conn, R.E.; Kolstad, J.J.; Borzelleca, J.F.; Dixler, D.S.; Filer, L.J.; Ladu, B.N.; Pariza, M.W. Safety assessment of polylactide (PLA) for use as a food-contact polymer. *Food Chem. Toxicol.* **1995**, *33*, 273–283. [CrossRef]
15. Siafaka, P.I.; Barmbalexis, P.; Bikiaris, D.N. Novel electrospun nanofibrous matrices prepared from poly(lactic acid)/poly(butylene adipate) blends for controlled release formulations of an anti-rheumatoid agent. *Eur. J. Pharm. Sci.* **2016**, *88*, 12–25. [CrossRef]
16. Freiberg, S.; Zhu, X.X. Polymer microspheres for controlled drug release. *Int. J. Pharm.* **2004**, *282*, 1–18. [CrossRef]
17. Park, S.-Y.; Pendleton, P. Mesoporous silica SBA-15 for natural antimicrobial delivery. *Powder Technol.* **2012**, *223*, 77–82. [CrossRef]
18. Farjadian, F.; Roointan, A.; Mohammadi-Samani, S.; Hosseini, M. Mesoporous silica nanoparticles: Synthesis, pharmaceutical applications, biodistribution, and biosafety assessment. *Chem. Eng. J.* **2019**, *359*, 684–705. [CrossRef]
19. Wang, Y.; Zhao, Q.; Han, N.; Bai, L.; Li, J.; Liu, J.; Che, E.; Hu, L.; Zhang, Q.; Jiang, T.; et al. Mesoporous silica nanoparticles in drug delivery and biomedical applications. *Nanomed. Nanotechnol. Biol. Med.* **2015**, *11*, 313–327. [CrossRef]

20. Nanaki, S.; Siafaka, P.I.; Zachariadou, D.; Nerantzaki, M.; Giliopoulos, D.J.; Triantafyllidis, K.S.; Kostoglou, M.; Nikolakaki, E.; Bikiaris, D.N. PLGA/SBA-15 mesoporous silica composite microparticles loaded with paclitaxel for local chemotherapy. *Eur. J. Pharm. Sci.* **2017**, *99*, 32–44. [CrossRef]

21. Vallet-Regi, M.; Rámila, A.; Del Real, R.P.; Pérez-Pariente, J. A new property of MCM-41: Drug delivery system. *Chem. Mater.* **2001**, *13*, 308–311. [CrossRef]

22. Gao, F.; Zhou, H.; Shen, Z.; Qiu, H.; Hao, L.; Chen, H.; Zhou, X. Synergistic antimicrobial activities of tea tree oil loaded on mesoporous silica encapsulated by polyethyleneimine. *J. Dispers. Sci. Technol.* **2020**, *41*, 1859–1871. [CrossRef]

23. Jin, L.; Teng, J.; Hu, L.; Lan, X.; Xu, Y.; Sheng, J.; Song, Y.; Wang, M. Pepper fragrant essential oil (PFEO) and functionalized MCM-41 nanoparticles: Formation, characterization, and bactericidal activity. *J. Sci. Food Agric.* **2019**, *99*, 5168–5175. [CrossRef] [PubMed]

24. Nanaki, S.; Tseklima, M.; Terzopoulou, Z.; Nerantzaki, M.; Giliopoulos, D.J.; Triantafyllidis, K.; Kostoglou, M.; Bikiaris, D.N. Use of mesoporous cellular foam (MCF) in preparation of polymeric microspheres for long acting injectable release formulations of paliperidone antipsychotic drug. *Eur. J. Pharm. Biopharm.* **2017**, *117*, 77–90. [CrossRef] [PubMed]

25. Nazzaro, F.; Fratianni, F.; De Martino, L.; Coppola, R.; De Feo, V. Effect of essential oils on pathogenic bacteria. *Pharmaceuticals* **2013**, *6*, 1451–1474. [CrossRef] [PubMed]

26. Devi, K.P.; Nisha, S.A.; Sakthivel, R.; Pandian, S.K. Eugenol (an essential oil of clove) acts as an antibacterial agent against Salmonella typhi by disrupting the cellular membrane. *J. Ethnopharmacol.* **2010**, *130*, 107–115. [CrossRef]

27. Ben Arfa, A.; Combes, S.; Preziosi-Belloy, L.; Gontard, N.; Chalier, P. Antimicrobial activity of carvacrol related to its chemical structure. *Lett. Appl. Microbiol.* **2006**, *43*, 149–154. [CrossRef]

28. Raut, J.S.; Karuppayil, S.M. A status review on the medicinal properties of essential oils. *Ind. Crops Prod.* **2014**, *62*, 250–264. [CrossRef]

29. Alkan Tas, B.; Sehit, E.; Erdinc Tas, C.; Unal, S.; Cebeci, F.C.; Menceloglu, Y.Z.; Unal, H. Carvacrol loaded halloysite coatings for antimicrobial food packaging applications. *Food Packag. Shelf Life* **2019**, *20*, 100300. [CrossRef]

30. Melendez-Rodriguez, B.; Figueroa-Lopez, K.J.; Bernardos, A.; Martínez-Máñez, R.; Cabedo, L.; Torres-Giner, S.; Lagaron, J.M. Electrospun Antimicrobial Films of Poly(3-hydroxybutyrate-co-3-hydroxyvalerate) Containing Eugenol Essential Oil Encapsulated in Mesoporous Silica Nanoparticles. *Nanomaterials* **2019**, *9*, 227. [CrossRef]

31. Majeed, H.; Bian, Y.-Y.; Ali, B.; Jamil, A.; Majeed, U.; Khan, Q.F.; Iqbal, K.J.; Shoemaker, C.F.; Fang, Z. Essential oil encapsulations: Uses, procedures, and trends. *RSC Adv.* **2015**, *5*, 58449–58463. [CrossRef]

32. Nerantzaki, M.; Kehagias, N.; Francone, A.; Fernández, A.; Sotomayor Torres, C.M.; Papi, R.; Choli-Papadopoulou, T.; Bikiaris, D.N. Design of a Multifunctional Nanoengineered PLLA Surface by Maximizing the Synergies between Biochemical and Surface Design Bactericidal Effects. *ACS Omega* **2018**, *3*, 1509–1521. [CrossRef] [PubMed]

33. Fernández, A.; Francone, A.; Thamdrup, L.H.; Johansson, A.; Bilenberg, B.; Nielsen, T.; Guttmann, M.; Sotomayor Torres, C.M.; Kehagias, N. Design of Hierarchical Surfaces for Tuning Wetting Characteristics. *ACS Appl. Mater. Interfaces* **2017**, *9*, 7701–7709. [CrossRef] [PubMed]

34. Lima, M.J.; Correlo, V.M.; Reis, R.L. Micro/nano replication and 3D assembling techniques for scaffold fabrication. *Mater. Sci. Eng. C* **2014**, *42*, 615–621. [CrossRef] [PubMed]

35. Papageorgiou, G.Z.; Palani, A.; Gilliopoulos, D.; Triantafyllidis, K.S.; Bikiaris, D.N. Mechanical properties and crystallization of high-density polyethylene composites with mesostructured cellular silica foam. *J. Therm. Anal. Calorim.* **2013**, *113*, 1651–1665. [CrossRef]

36. Zhao, D.; Huo, Q.; Feng, J.; Chmelka, B.F.; Stucky, G.D. Nonionic triblock and star diblock copolymer and oligomeric sufactant syntheses of highly ordered, hydrothermally stable, mesoporous silica structures. *J. Am. Chem. Soc.* **1998**, *120*, 6024–6036. [CrossRef]

37. Karakoulia, S.A.; Triantafyllidis, K.S.; Lemonidou, A.A. Preparation and characterization of vanadia catalysts supported on non-porous, microporous and mesoporous silicates for oxidative dehydrogenation of propane (ODP). *Microporous Mesoporous Mater.* **2008**, *110*, 157–166. [CrossRef]

38. Papadopoulos, L.; Klonos, P.A.; Terzopoulou, Z.; Psochia, E.; Sanusi, O.M.; Hocine, N.A.; Benelfellah, A.; Giliopoulos, D.; Triantafyllidis, K.; Kyritsis, A.; et al. Comparative study of crystallization, semicrystalline morphology, and molecular mobility in nanocomposites based on polylactide and various inclusions at low filler loadings. *Polymer (Guildf.)* **2021**, *217*, 123457. [CrossRef]

39. John, J.; Tang, Y.; Rothstein, J.P.; Watkins, J.J.; Carter, K.R. Large-area, continuous roll-to-roll nanoimprinting with PFPE composite molds. *Nanotechnology* **2013**, *24*. [CrossRef]

40. Khang, D.Y.; Lee, H.H. Sub-100 nm Patterning with an Amorphous Fluoropolymer Mold. *Langmuir* **2004**, *20*, 2445–2448. [CrossRef]

41. Mann, E.E.; Manna, D.; Mettetal, M.R.; May, R.M.; Dannemiller, E.M.; Chung, K.K.; Brennan, A.B.; Reddy, S.T. Surface micropattern limits bacterial contamination. *Antimicrob. Resist. Infect. Control* **2014**, *3*. [CrossRef] [PubMed]

42. Rouquerol, J.F.; Rouquerol, K.S.W.; Sing, P.L.; Aix, G.M. *Adsorption by Powders and Porous Solids Principles, Methodology and Applications*; Academic Press: Cambridge, UK, 2014; ISBN 9780080970356.

43. Zhang, Y.; Jiang, T.; Zhang, Q.; Wang, S. Inclusion of telmisartan in mesocellular foam nanoparticles: Drug loading and release property. *Eur. J. Pharm. Biopharm.* **2010**, *76*, 17–23. [CrossRef] [PubMed]

44. Macina, D.; Piwowarska, Z.; Tarach, K.; Góra-Marek, K.; Ryczkowski, J.; Chmielarz, L. Mesoporous silica materials modified with alumina polycations as catalysts for the synthesis of dimethyl ether from methanol. *Mater. Res. Bull.* **2016**. [CrossRef]

45. Aktas, O.; Yasyerli, S.; Dogu, G.; Dogu, T. Structural variations of MCF and SBA-15-like mesoporous materials as a result of differences in synthesis solution pH. *Mater. Chem. Phys.* **2011**, *131*, 151–159. [CrossRef]

46. Johansson, E.M.; Córdoba, J.M.; Odén, M. The effects on pore size and particle morphology of heptane additions to the synthesis of mesoporous silica SBA-15. *Microporous Mesoporous Mater.* **2010**, *133*, 66–74. [CrossRef]

47. Ji, X.; Hampsey, J.E.; Hu, Q.; He, J.; Yang, Z.; Lu, Y. Mesoporous Silica-Reinforced Polymer Nanocomposites. *Chem. Mater.* **2003**, *15*, 3656–3662. [CrossRef]

48. Klonos, P.; Terzopoulou, Z.; Koutsoumpis, S.; Zidropoulos, S.; Kripotou, S.; Papageorgiou, G.Z.; Bikiaris, D.N.; Kyritsis, A.; Pissis, P. Rigid amorphous fraction and segmental dynamics in nanocomposites based on poly(L–lactic acid) and nano-inclusions of 1–3D geometry studied by thermal and dielectric techniques. *Eur. Polym. J.* **2016**, *82*, 16–34. [CrossRef]

49. Rittigstein, P.; Priestley, R.D.; Broadbelt, L.J.; Torkelson, J.M. Model polymer nanocomposites provide an understanding of confinement effects in real nanocomposites. *Nat. Mater.* **2007**, *6*, 278–282. [CrossRef]

50. Terzopoulou, Z.; Klonos, P.A.; Kyritsis, A.; Tziolas, A.; Avgeropoulos, A.; Papageorgiou, G.Z.; Bikiaris, D.N. Interfacial interactions, crystallization and molecular mobility in nanocomposites of Poly(lactic acid) filled with new hybrid inclusions based on graphene oxide and silica nanoparticles. *Polymer (Guildf.)* **2019**, *166*, 1–12. [CrossRef]

51. Papadopoulos, L.; Terzopoulou, Z.; Vlachopoulos, A.; Klonos, P.A.; Kyritsis, A.; Tzetzis, D.; Papageorgiou, G.Z.; Bikiaris, D. Synthesis and characterization of novel polymer/clay nanocomposites based on poly(butylene 2,5-furan dicarboxylate). *Appl. Clay Sci.* **2020**, *190*, 105588. [CrossRef]

52. Jobdeedamrong, A.; Jenjob, R.; Crespy, D. Encapsulation and Release of Essential Oils in Functional Silica Nanocontainers. *Langmuir* **2018**, *34*, 13235–13243. [CrossRef] [PubMed]

53. Kim, S.; Jung, U.T.; Kim, S.-K.; Lee, J.-H.; Choi, H.S.; Kim, C.-S.; Jeong, M.Y. Nanostructured Multifunctional Surface with Antireflective and Antimicrobial Characteristics. *ACS Appl. Mater. Interfaces* **2015**, *7*, 326–331. [CrossRef] [PubMed]

54. Ranjbar-Mohammadi, M.; Bahrami, S.H.; Joghataei, M.T. Fabrication of novel nanofiber scaffolds from gum tragacanth/poly(vinyl alcohol) for wound dressing application: In vitro evaluation and antibacterial properties. *Mater. Sci. Eng. C* **2013**, *33*, 4935–4943. [CrossRef]

55. Dickson, M.N.; Liang, E.I.; Rodriguez, L.A.; Vollereaux, N.; Yee, A.F. Nanopatterned polymer surfaces with bactericidal properties. *Biointerphases* **2015**, *10*, 021010. [CrossRef] [PubMed]